Effects of reactive dissolution of orthopyroxene in producing incompatible element depleted melts and refractory mantle residues during early fore-arc spreading: constraints from ophiolites in eastern Mediterranean

Ercan Aldanmaz [a,*], Douwe J.J. van Hinsbergen [b], Özlem Yıldız-Yüksekol [a], Max W. Schmidt [c], Peter J. McPhee [b], Thomas Meisel [d], Aykut Güçtekin [a], Paul R.D. Mason [b]

[a] Department of Geology, University of Kocaeli, Izmit 41040, Turkey
[b] Department of Earth Sciences, University of Utrecht, Budapestlaan 4, 3584 CD Utrecht, The Netherlands
[c] Institute of Mineralogy and Petrology, ETH, 8092 Zurich, Switzerland
[d] Department of General and Analytical Chemistry, Montanuniversität Leoben, Franz-Josef-Str. 18, A-8700 Leoben, Austria

ARTICLE INFO

ABSTRACT

Compositional variations of peridotites from the Cretaceous ophiolites in southern Turkey and Northern Cyprus are presented to document the nature of partial melting and possible effects of reactive dissolution of primary mantle phases during fore-arc spreading. The peridotites overall exhibit a range of $^{187}Os/^{188}Os$ ratios from 0.1171 to 0.1266 and appear to represent a mantle region that preserves a record of ancient melt depletion. The samples are depleted in $^{187}Os/^{188}Os$ compared to the ambient oceanic upper mantle ($^{187}Os/^{188}Os$ ~0.127), suggesting that they are representatives of a shallow fore-arc mantle where transport of radiogenic ^{187}Os during slab dehydration was limited. Chemical variations of primary mantle minerals indicate that the peridotites are the residues of moderate to high degrees (>16%) of partial melting and have experienced significant modal and chemical compositional modification through interaction with oxidizing hydrous basaltic melts. Interacting melts, which appear to be similar in composition to primitive arc tholeiite, are likely to have originated from sub-lithospheric lower part of the mantle wedge during early stages of fore-arc spreading and migrated upward to react with variably depleted harzburgites to induce further melting in the overlying lithospheric mantle through open-system reactive flow. This second stage melting resulted in (1) common occurrence of reactive harzburgites and dunites by incongruent melting of orthopyroxene and crystallization of olivine through interaction with olivine saturated melt; and (2) local development of refertilized peridotites by shallower melt impregnation that involves interaction with olivine + clinopyroxene saturated melt. The dissolution of orthopyroxene caused the reacting melt to be enriched in silica and diluted in incompatible elements which led to the production of the final melts similar in composition to fore arc basalt and boninite. Involvement of compositionally variable mantle and melt components with different rates of melt influx therefore appears to explain the generation of fore-arc crust with a range of diverse rock suites including temporally and spatially associated arc tholeiites and boninites with significant depletion in incompatible elements.

© 2020 Elsevier B.V. All rights reserved.

1. Introduction

Peridotites from ophiolite suites are generally interpreted to largely represent solid residues that were left behind following variable degrees of melt extraction during oceanic crust formation. Compositional variations in these mantle relicts provide insights into tectonic processes operating along plate boundaries, and record the history of large-scale magmatic events that include partial melting, melt movement and fluid-mantle interaction (e.g., Aldanmaz et al., 2009; Birner et al., 2017; Parkinson and Pearce, 1998).

Lithospheric mantle beneath oceanic regions may form in either mid-oceanic ridge settings or spreading centers above subduction systems (e.g., Stern et al., 2012; van Hinsbergen et al., 2015). Distinct behaviors of melt generation in these tectonic settings are signified by specific mineralogical and chemical signatures that are reflected in the compositions of the melt products and complementary solid residues of mantle melting (Aldanmaz et al., 2009; Arai, 1994; Hellebrand et al., 2001; Johnson et al., 1990; O'Driscoll et al., 2015). Mineralogical and

chemical compositional variations in mantle rocks within lithospheric relicts, moreover, are largely the results of an array of complex processes including metasomatic alterations through interaction of residues with percolating melts (Kelemen et al., 1992, 1997; Niu, 2004; O'Driscoll et al., 2015).

The ophiolite suites in Southern Turkey, NW Arabia, and Cyprus are dispersed as isolated bodies that rest as klippen on continental margin rocks, or microcontinent-derived nappes (Fig. 1). These represent the remains of oceanic lithosphere that was once located in the supra-slab regions of Late Cretaceous intra-oceanic subduction zones. The oceanic lithosphere was obducted when passive continental margins of eastern Mediterranean continental fragments arrived at the trench (Maffione et al., 2017; Moix et al., 2008; Robertson, 2002), and led to the formation of a complex mosaic of ophiolitic klippen across the orogen (Maffione et al., 2017; Moix et al., 2008; van Hinsbergen et al., 2016). Paleomagnetic and kinematic reconstructions suggest that these forearc ophiolites formed at ~N-S trending ridges in the upper plate of, and parallel to intra-oceanic subduction zones that were affected by roll-back. Based mainly on geochemical data from melt products forming the crustal sequences, previous studies have highlighted the supra subduction zone (SSZ)-type nature of these ophiolites (Bağcı et al., 2005; Dilek and Thy, 2009; Parlak et al., 2013), and geochronological analyses demonstrate that ophiolitic crust in the Eastern Mediterranean region consistently yielded ages within a short time span of ~93–90 Ma (Maffione et al., 2017; Robertson, 2002). Ophiolites of the southern Taurides, Cyprus, and NW Arabia likely formed part of a radially expanding, westward retreating Late Cretaceous intra-oceanic subduction zone that obducted northward onto the southern Anatolian margin, and south- and southeastward onto the north African margin (Cyprus) and the northern Arabian margin (Maffione et al., 2017; McPhee and Van Hinsbergen, 2019; Moix et al., 2008; van Hinsbergen et al., 2020).

The ophiolite bodies in this region have the potential to provide insights into the petrological processes that are operational in creating compositional heterogeneities in supra-slab mantle regions. In particular, the existence of rock suites with contrasting petrological affinities in both the crustal and mantle portions of these ophiolites may provide the most compelling evidence that the compositional variations in these ophiolites reflect distinct stages of oceanic lithosphere generation in different parts of a subduction system.

Here, we examine the geochemical characteristics of ultramafic rocks from the ophiolite complexes of southern Turkey and northern Cyprus in an attempt to provide constraints on the possible effects of subduction-derived melts in shaping the composition of mantle lithosphere during early fore-arc spreading. We particularly focus on identifying the differential effects of compositionally distinct types of melts that interact with solid residue to generate compositional heterogeneities in different parts of a supra-slab mantle zone.

2. Geological setting

Convergence between Eurasia and Africa/Arabia during the Mesozoic led to the development of a large accretionary orogen, most of which formed when continental lithosphere arrived in trenches below continental or oceanic lithosphere in the upper plate. In case of the latter, this leads to widespread emplacement of oceanic lithospheric fragments onto the passive continental margins, forming ophiolites. Ophiolite complexes across the circum-Mediterranean region formed due to intra-oceanic subduction within Neotethyan oceanic basins, and formed in the Jurassic and Late Cretaceous (Fig. 1a) (Maffione et al., 2017; Robertson, 2002). Geochemical and petrological data from these ophiolites indicate that they are mainly of supra-subduction zone (SSZ)-type (Dilek and Thy, 2009; Parlak et al., 1996) and likely formed shortly after subduction initiation along fracture zones within the Neotethys ocean (Maffione et al., 2017).

Cretaceous SSZ ophiolites in Anatolia are organized in two main belts that were emplaced during intra-oceanic subduction in different oceanic basins separated by a continental domain with platforms and intervening deep oceanic basins, that rifted from Gondwana in Paleozoic or Early Mesozoic time known as the Adria-Turkey plate (e.g., Stampfli et al., 1991). A series of ophiolites in Turkey is found overlying the Cretaceous to Eocene Anatolide-Tauride fold-thrust belt and are thought to result from at least one, north and east dipping intra-oceanic subduction system (Maffione et al., 2017; Robertson, 2002; van Hinsbergen et al., 2016). A second belt contains the peri-Arabian ophiolites, obducted onto the Arabian continent in latest Cretaceous time (e.g., Al-Riyami et al., 2002). The belt of peri-Arabian ophiolites include the Kızıldağ (or Hatay) ophiolite of SE Anatolia, the Baer Bassit ophiolite of Syria, and likely extends westward toward the famous Troodos ophiolite of southwestern Cyprus, which was emplaced southwards onto the Arabian and African passive margin in the Late Cretaceous (e.g.,Maffione et al., 2017 ; McPhee and Van Hinsbergen, 2019). This belt also includes several ophiolites that were thrusted northward onto the southern Taurides to the north of Cyprus, including the ophiolites overlying the Antalya-Alanya nappes, and likely also the Mersin ophiolite (Fig. 1) (Maffione et al., 2017; Morris et al., 2017). The simultaneous northward and southward ophiolite obduction of the peri-Arabian-Cyprus-southern Tauride belt followed a westward, radial roll-back event that involved major rotations of the ophiolites (e.g., Maffione et al., 2017; Moix et al., 2008).

The main characteristics of the ophiolite suites studied different localities in southern Turkey and northern Cyprus have been described in some detail (e.g. Morris et al., 2017; Parlak et al., 2013; Robertson, 2002) and only some brief information will be presented here on the ophiolite localities selected for our study come from the east (Kızıldağ), south (Kyrenia Range), and north (Mersin) of the southern belt, which restore to the northern (Mersin), central (Kyrenia Range) and southern (Kızıldağ) part of an east-dipping intra-oceanic subduction zone around ~90 Ma (Maffione et al., 2017; McPhee and Van Hinsbergen, 2019) (Fig. 2).

2.1. Kızıldağ ophiolite

The Kızıldağ ophiolite in southern Turkey, which is one of the best preserved exposures among the Eastern Mediterranean ophiolites, was thrust upon NW Arabia in the Late Cretaceous, and comprises a near complete ophiolite succession with well-developed mantle and crustal sequences (Fig. 1b) (Bağcı et al., 2005; Karaoğlan et al., 2013). On the basis of zircon U—Pb geochronologic data, Dilek and Thy (2009) and Karaoğlan et al. (2013) identified a time span of 91–92 Ma for the formation of the crystalline crustal sequence of the ophiolite. The tectonic emplacement of the suite onto the Arabian continent occurred earlier than Maastrichtian and after Turonian based on the ages of the youngest sediments below, and the oldest sediments sealing the obduction thrust (Dilek and Thy, 2009; Karaoğlan et al., 2013). The Kızıldağ ophiolite succession consists of tectonized peridotites, a cumulate sequence of mafic and ultramafic rocks, massive gabbro, a sheeted dyke complex, plagiogranite and an extrusive complex (Bağcı et al., 2005; Dilek and Thy, 2009). The mantle section of the suite is represented mainly by harzburgites with locally developed patches of dunite, while wehrlite, olivine gabbro and gabbro are the main rock types in the cumulate sequence. The extrusive part is composed largely of basaltic rocks with typical island arc tholeiite geochemical affinities, although low-Ti extrusive rocks that are known as 'sakalavites' have also been reported (Bağcı et al., 2005; Dilek and Thy, 2009).

2.2. Mersin ophiolite

The Mersin ophiolite is positioned on the southern Tauride fold-thrust belt in southern Turkey (Fig. 1c). It consists of mantle tectonites, ultramafic and mafic cumulates (pyroxenite and layered gabbro), massive gabbro and subordinate basaltic lavas associated with pelagic sediments (Parlak et al., 1996). Discrete dolerite dykes that cut through the
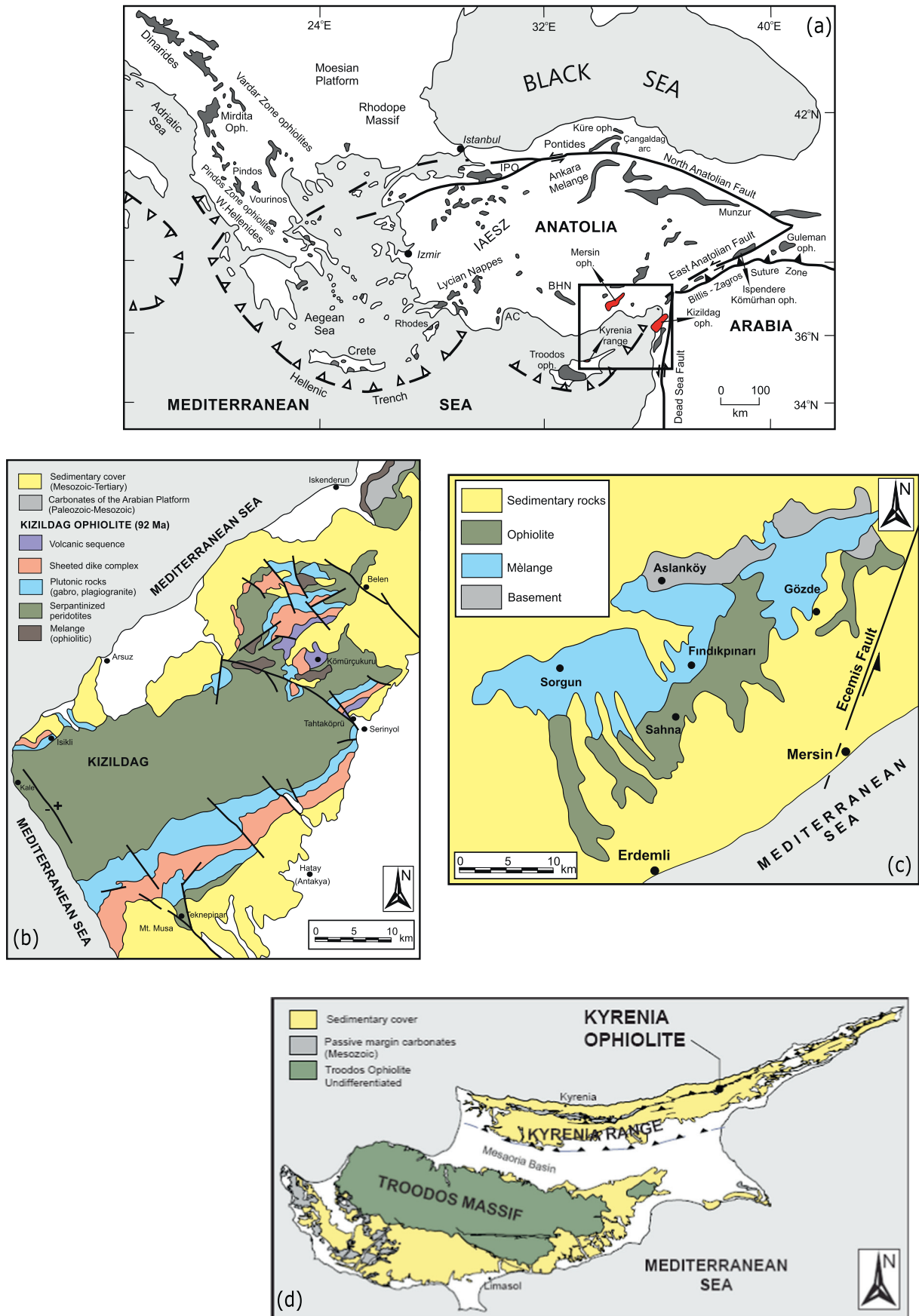
Fig. 1. (a) Tectonic map showing the distribution of Neotethyan ophiolites of the Eastern Mediterranean region (modified from Robertson, 2002), with simplified maps for the key sampling localities for the ophiolites. Maps for (b) the Kızıldağ ophiolite, (c) the Mersin ophiolite; and (d) the Kyrenia range are modified from Dilek and Thy (2009), Parlak et al. (1996), and Robertson et al. (2013), respectively. *Key to abbreviations:* AC = Antalya Complex; BHN = Beysehir-Hoyran Nappes; IAESZ = Izmir-Ankara-Erzincan Suture Zone.

Fig. 2. Paleogeographic reconstruction of the eastern Mediterranean Neotethys at the time of suprasubduction zone ophiolite formation (~92 Ma) showing the areas of continental and oceanic crust and the main subduction zones (modified from Maffione et al., 2017 and van Hinsbergen et al., 2020).

tectonized harzburgites are found in some localities, although a typical sheeted dyke complex is absent. The ophiolitic sequence includes a locally preserved sub-ophiolitic metamorphic sole, and rests on a mélange. $^{40}Ar/^{39}Ar$ isotopic dating of metamorphic sole rocks from the Mersin ophiolite yield a Late Cretaceous age (91–94 Ma; Thuizat et al., 1981; Parlak and Delaloye, 1999). Morris et al. (2017) showed that the ophiolite underwent a first phase of magmatic spreading, followed by tectonic extension accommodated along oceanic detachment faults, both before and after the welding of the metamorphic sole to the ophiolite's mantle section. The absence of a significant crustal sequence is thus likely the result of the very high extensional fragmentation of the ophiolite (e.g., van Hinsbergen et al., 2015). Kinematic indicators in the metamorphic sole and underlying carbonates indicate a northward ophiolite emplacement direction (Parlak et al., 1996), although some researchers also suggest southward initial emplacement of this ophiolite (e.g., Parlak and Robertson, 2004). The presence of Carboniferous and younger radiolarian cherts in the mélange below the Mersin ophiolite suggests that Carboniferous or older crust subducted below the Mersin ophiolite prior to its obduction (Moix et al., 2011; Sayit et al., 2017; Tekin et al., 2019).

2.3. Kyrenia range ophiolite

A suite of ophiolitic rocks is exposed for ~1 km along the NE Kyrenia range of Cyprus, near the village of Kantara (Fig. 1d). The suite is part of a middle Eocene olistostrome (Robertson et al., 2013) that covers low grade metamorphic carbonates known as the Trypa group. It consists of a dismembered body of 10–100 m sized ophiolite blocks, which are interspersed with a chaotic matrix that contains clasts of chert, fine grained limestone, dolerite and pelagic limestone in a sandy matrix. The underlying Trypa group carbonates are interpreted to have been metamorphosed by obduction below ophiolite, and then exhumed to the sea floor by extension in Late Cretaceous times (McPhee and van Hinsbergen, 2019). The Ophiolite at Kantara is likely a locally derived remnant of the hanging wall in the extension system that exhumed the Trypa group and forms an outlier of the more extensive Troodos ophiolite in the south.

3. Peridotite petrography

The rocks we analyzed are from the mantle portions of the three ophiolite suites described above. The mantle parts of these lithospheric relicts exhibit some similarities in terms of modal compositions and petrography. They are composed largely of harzburgite, generally interpreted to represent melt-depleted residue left behind following variable degrees of partial melting of a lherzolite source. Variable amounts of dunites are also observed, mainly as discordant lenses or bands hosted in the large harzburgite bodies within the Kızıldağ and Mersin ophiolites. Dunite lenses in some cases also contain abundant chromite deposits.

The harzburgites from all three suites are variably serpentinized with the modal extent of serpentinization ranging from ~35 and 50% for the Kızıldağ, ~40 and 65% for the Mersin, and 60 and 80% for the Kyrenia range ophiolites. The samples commonly display medium to coarse grained porphyroclastic textures, although there are also some samples in the Kızıldağ suite exhibiting protogranular textures. The porphyroclastic types consist of olivine (~75–85 vol%), orthopyroxene (~15–25 vol%) and minor clinopyroxene (<5 vol%). Large olivine porphyroclasts are generally elongated and show strain lamellae, although polygonal neoblasts of smaller olivine grains are also present in some of the samples. Orthopyroxenes generally form discrete large crystals that are often surrounded by smaller grains of olivine. They commonly display undulatory extinction with curving cleavage. The clinopyroxene is usually found as discrete small crystals with curvilinear borders, most commonly occupying interstitial spaces. Holly leaf-shaped brown spinel represents the primary accessory phase (up to 3%) in most of the samples. It forms as anhedral and subhedral grains with curvilinear crystal margins, or in some cases, as subhedral crystals at olivine grain boundaries. In some of the highly serpentinized samples, chromium-rich spinels display rims of magnetite or chromian magnetite that appear to have developed during hydrothermal alteration.

The samples with protogranular texture in the Kızıldağ suite are typical with their smooth, curved grain boundaries, and commonly show signs of weak deformation, while the dunites that form as discordant patches within the harzburgite generally have coarse grained granular textures. The dunites are relatively less serpentinized (<30%) and exhibit porphyroclastic and disrupted mylonitic fabrics, with fine grained olivine and disseminated spinel.

4. Geochemistry

4.1. Analytical techniques

Whole-rock major and trace element analyses were carried out at the Montanuniversität Leoben (Austria) using the methods described in Aldanmaz et al. (2012). In brief, powdered rock samples were first dried at 110 °C and heated to 950 °C for ~2 h to determine loss on ignition. Ignited powders and $Li_2B_4O_7$ were used to prepare fused glass disks on which major element concentrations were determined with a wavelength dispersive X-ray fluorescence spectrometer (ARL Fisons Instruments 8410). Reproducibility, based on repeated analyses of samples and standards (UB-N, PCC-1), was better than (RSD in%) 0.21 for SiO_2, 0.90 for TiO_2, 1.31 for MnO, 0.52 for Al_2O_3, 0.23 for Fe_2O_3, 0.31 for MgO, 0.88 for CaO, 3.11 for Na_2O, 8.28 for V, 2.17 for Ni, 1.14 for Co and 3.28 for Cu.

Major element analyses of olivines, pyroxenes and spinels for some of the ultramafic rocks were carried out in ETH Zurich using a JEOL JXA-8200 microprobe, while an additional set of samples were analyzed on a JEOL Superprobe 8600 at Utrecht University. Operating conditions during measurements for both set of analyses were 15 kV accelerating voltage, 20 nA beam current and 20–100 s counting time. Synthetic and natural mineral standards were used to obtain reliable results.

A subset of samples was prepared for in-situ measurements of clinopyroxene and spinel trace element concentrations using the approach defined in Aldanmaz et al. (2009). The analyses were carried out on >80 μm-thick polished sections using LA-ICP-MS at ETH Zurich.

Ablation was performed in a helium atmosphere using an ArF Excimer laser (193 nm) with a pulse energy of 100 mJ and a pulse repetition rate of 5 Hz. The ablated material was flushed in a continuous argon flow into the torch of an ELAN 6100 DRC ICP-MS. Repeat analysis of external standard (NIST SRM 610) was performed between analyses of 10 unknowns for linear drift correction. ^{43}Ca and ^{30}Si from electron microprobe analyses were used as internal standards. The values reported are the average of 3 to 10 analyses for each mineral grain.

Os and Re abundances and $^{187}Os/^{188}Os$ ratios were measured at the Montanuniversität Leoben on a quadrupole ICPMS (HP 7500, Agilent Technologies) by applying the isotope dilution method (see Aldanmaz et al., 2012 for details). In brief, rock powders were weighed with a spike solution consisting of HSE isotope traces and dissolved using a mixture of 5 ml HNO_3 and 2 ml HCl in quartz vessel in a high-pressure asher at 300 °C and 125 bar. Osmium concentrations and $^{187}Os/^{188}Os$ were determined directly via sparging OsO_4 into the mass spectrometer, while Re concentrations were measured from the residue, for which the solution was centrifuged and dried before being re-dissolved in 2 ml of 0.1 mol/l HCl. External reproducibility, based on repeat analyses of the in-house reference material (LOsST), was better than ±2.4‰ at the 2σ level for $^{187}Os/^{188}Os$. Osmium and Re concentrations from several repeat analyses of the reference material (UB-N) were in the range reported by Meisel et al. (2003), indicating an uncertainty of <10% (2RSD).

4.2. Bulk-rock compositions

Because the samples we use are variably serpentinized peridotites, we consider it unlikely that their trace element abundances are representative of pre-serpentinization magmatic processes. Thus, in order to evaluate the bulk-rock compositional variations we concentrate on major element abundances which are not significantly affected by serpentinization processes (e.g., Niu, 2004). The mantle representatives from all three ophiolite suites display a limited range of MgO from 44 to 49 wt% (Fig. 3). The MgO abundances of the peridotites increase with decreasing modal abundance of clinopyroxene and may reflect the degree of melt depletion. Bulk-rock compositions exhibit progressive trends of depletions in incompatible elements (e.g., Al, Ca and Ti) with increasing MgO contents of the samples (Fig. 3). Concentrations of CaO and Al_2O_3 range from 1.38 to 0.23 and from 1.47 to 0.85 wt%, respectively, indicating that the rocks represent a mantle region that is more depleted than the average MORB source composition (Fig. 3). In the majority of the samples these depletions in fusible components are accompanied by an increase of the modal abundance of olivine, suggesting that the peridotites may have been formed as melting residues. In a number of samples, however, the relatively higher FeO values and the steeper SiO_2–MgO trends than expected for residues of partial melting may indicate additional effects of melt – rock interaction.

Although the ultramafic rock suites sampled during the course of this study represent melt-depleted mantle regions, there appear to be some clear distinctions between the ophiolite bodies in terms of their major element relative abundances. The Mersin ophiolite, for instance, is remarkable for its relatively more depleted mantle section as the peridotites sampled from this suite have higher MgO and lower CaO and Al_2O_3 abundances than those from the other two suites (Fig. 3).
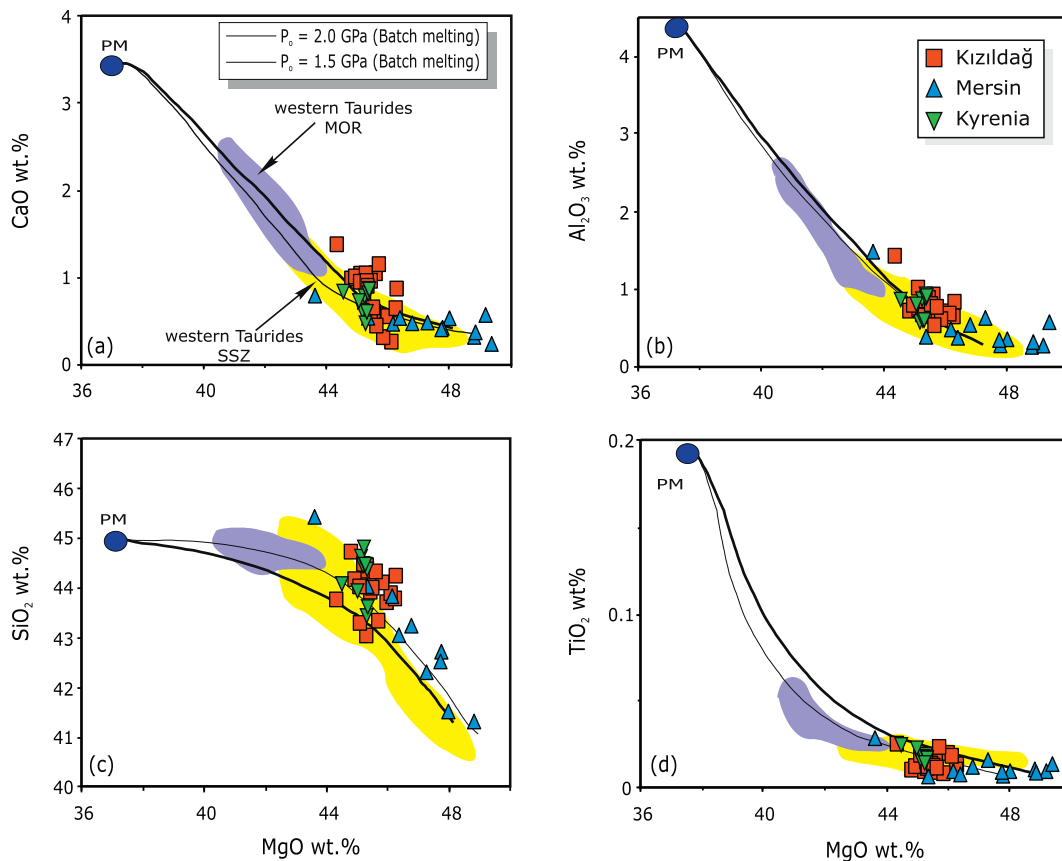

Fig. 3. (a to d) Variations of bulk-rock CaO, Al_2O_3, TiO_2, and SiO_2 with MgO for the peridotites. The curves represent the theoretically calculated compositions of melting residues obtained using incrementally isentropic polybaric fractional melting method based on the parameters described in Asimow (1999). Also plotted for comparison are the compositional fields for the peridotites from western Tauride ophiolites (shown as Lycian and Antalya ophiolites in Fig. 1a). Western Tauride ophiolite compositional fields are based on the data from Aldanmaz et al. (2009).

4.3. Mineral chemistry of primary mantle phases

4.3.1. Major oxide variations

Olivine is the most abundant component in all peridotites examined in this study. The olivine is compositionally homogeneous and rich in Mg, with Mg# values ranging from 0.906 to 0.917. Although the analyzed grains from all three sampling suites display some compositional similarities, olivines in the Mersin samples have lower Mg# than those in the other two suites, possibly indicating secondary crystallization of lower forsteritic olivine by reactive flow. The NiO and MnO contents of olivines range from 0.11 to 0.43 and from 0.09 to 0.18 (in wt%), respectively, and are comparable to those of olivines from highly depleted residues in ophiolite suites worldwide (e.g. Aldanmaz et al., 2009; Arai, 1994).

Orthopyroxene is the second most abundant primary silicate in the peridotites and is represented by enstatite. The Mg# values of orthopyroxenes range from 0.909 to 0.920 and increase with increasing Mg# of olivines, indicating that they were in chemical equilibrium. Orthopyroxenes are in general characterized by very low abundances of Al_2O_3, TiO_2 and Na_2O and their Cr# values range from 0.39 to 0.90 wt%.

Clinopyroxene is represented by diopside and shows a relatively wide range of Mg# between 0.923 and 0.947. There is a significant difference between the sampled suites in terms of clinopyroxene compositions. Diopsites from the Kızıldağ ophiolite are characterized by lower Mg# compared to those from the other two suites, although similar compositional distinction is not observed in the Mg# of olivines or orthopyroxenes. Clinopyroxenes have low abundances of TiO_2 (< 0.22 wt%), Na_2O (< 0.24 wt%) and Al_2O_3 (< 3.05 wt%) and the increasing abundances in these elements correlate with decreasing Mg#.

The spinels are all Cr-rich with their high Cr# values [$Cr/(Cr + Al)$] that range from 0.47 to 0.75. Their compositions are comparable to spinels in peridotites from supra-subduction zone (SSZ) ophiolites and those from convergent margins (Aldanmaz, 2012; Dick and Bullen, 1984; Parkinson and Pearce, 1998). The TiO_2 content of the spinels displays significant variation from 0.01 to 0.47 (wt%) and generally increases with increasing Cr#.

Ratios of Cr/Al in spinel and Fe/Mg in olivine from mantle residues are generally considered to be indicators of the degree of partial melting because continuous melt extraction is known to gradually deplete the residual phases in more incompatible elements (Dick and Bullen, 1984). Thus, Cr/Al ratio of spinel and Mg/Fe ratio of olivine increase progressively with ongoing partial melting and depletion, defining the residual peridotite array on a plot of olivine Mg# vs. spinel Cr# (e.g., Arai, 1994). Variations of spinel compositions with those of coexisting olivines for the peridotites investigated here are illustrated in Fig. 4 where the samples all plot within the residual peridotite array. Although the samples from three individual suites occupy different parts of the array, they have a compositional range reflecting partial melting in a supra-slab mantle region.

4.3.2. Clinopyroxene trace element abundances

Clinopyroxenes analyzed in-situ by LA-ICP-MS have variable trace element patterns. On a chondrite-normalized plot the majority of the samples are characterized by LREE relative depletions (Fig. 5). This type of REE pattern is common in clinopyroxenes from abyssal peridotites and some tectonized peridotites from ophiolites, and is usually interpreted to signify the effects of melt removal which deplete the residue in more incompatible elements to a greater degree (e.g., Aldanmaz et al., 2009; Bizimis et al., 2000; Johnson et al., 1990). The majority of clinopyroxene grains have lower HREE absolute abundances than the compositional range for the abyssal peridotites, possibly indicating that they have experienced greater extent of melt extraction than those originated in a typical mid-ocean ridge setting (Fig. 5).

In terms of LREE abundances the clinopyroxenes display significant variations (Fig. 5). Some of the samples are depleted in LREE/MREE
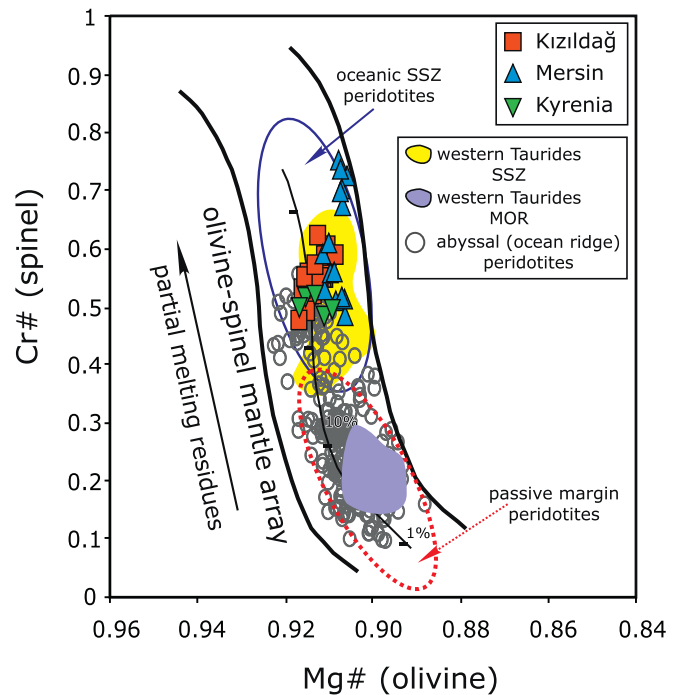

Fig. 4. Diagram showing the variations of olivine Mg# with spinel Cr# for the peridotites. The compositional fields for ocean ridge peridotites, oceanic arc peridotites, and passive continental margin peridotites are from Dick and Bullen, (1984) and (Pearce et al., 2000). The olivine-spinel mantle array and melting trend are from Arai (1994).

ratios, which can be related to continuous melt removal, while some others are characterized by slightly elevated LREE concentrations. The latter possibly indicates metasomatic enrichments during which trace elements with higher incompatibility are redistributed more efficiently. Clinopyroxenes from all three suites have low abundances of high-field-strength elements (HFSE); their Zr and Ti concentrations range between 0.12 and 1.67 ppm and 101–1371 ppm, respectively.

The peridotites from the three individual suites display some variability in terms of the relationships between clinopyroxene trace element contents and melt depletion indices. The samples from the Mersin suite, for instance, exhibit an apparent negative correlation between clinopyroxene Yb content and spinel Cr#, while those from the Kızıldağ suite are characterized by a more scattered distribution with some of the samples having greater Yb contents than estimated for simple melt residues (Fig. 6). The former is probably a reflection of continuous melt depletion, which removes the more incompatible elements more efficiently generating a depletion trend similar to the theoretically calculated melting trajectory shown in Fig. 6, while the latter is likely the result of REE enrichments by melt impregnation.

4.4. Osmium isotopic variations

Osmium isotope data are presented for the samples from the Kızıldağ and Mersin ophiolites. The $^{187}Os/^{188}Os$ ratios of the peridotites from these two ophiolites display large variations ranging from 0.1171 to 0.1266. The samples generally have lower $^{187}Os/^{188}Os$ ratios than the mean present-day chondritic value (0.1270; Luck and Allègre, 1983) and the commonly accepted value of primitive upper mantle (0.1296; e.g., Meisel et al., 1996), indicating that they represent a mantle region that had experienced long-term $^{187}Re/^{188}Os$ depletion. They display no clear co-variance of $^{187}Os/^{188}Os$ with Os abundances or melt depletion indices such as Al_2O_3 contents (Fig. 7). With their γOs values ranging between −7.7 to −0.2 the peridotites are generally more depleted than the estimated depleted MORB source (e.g., Salters and

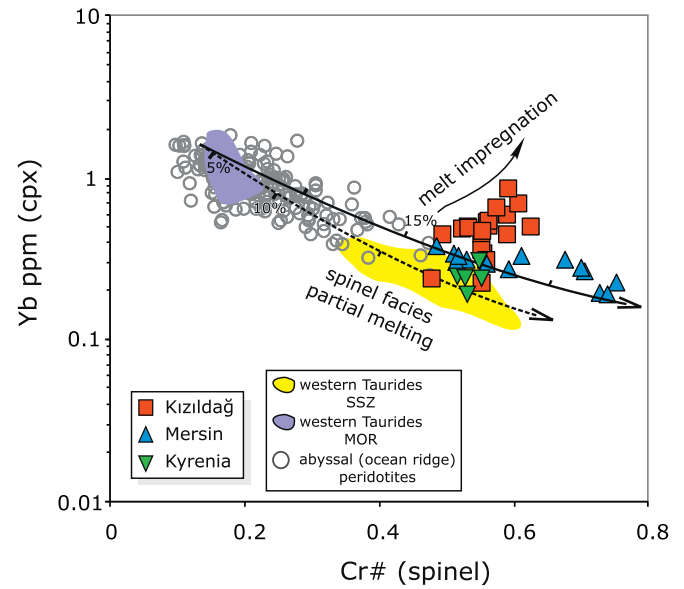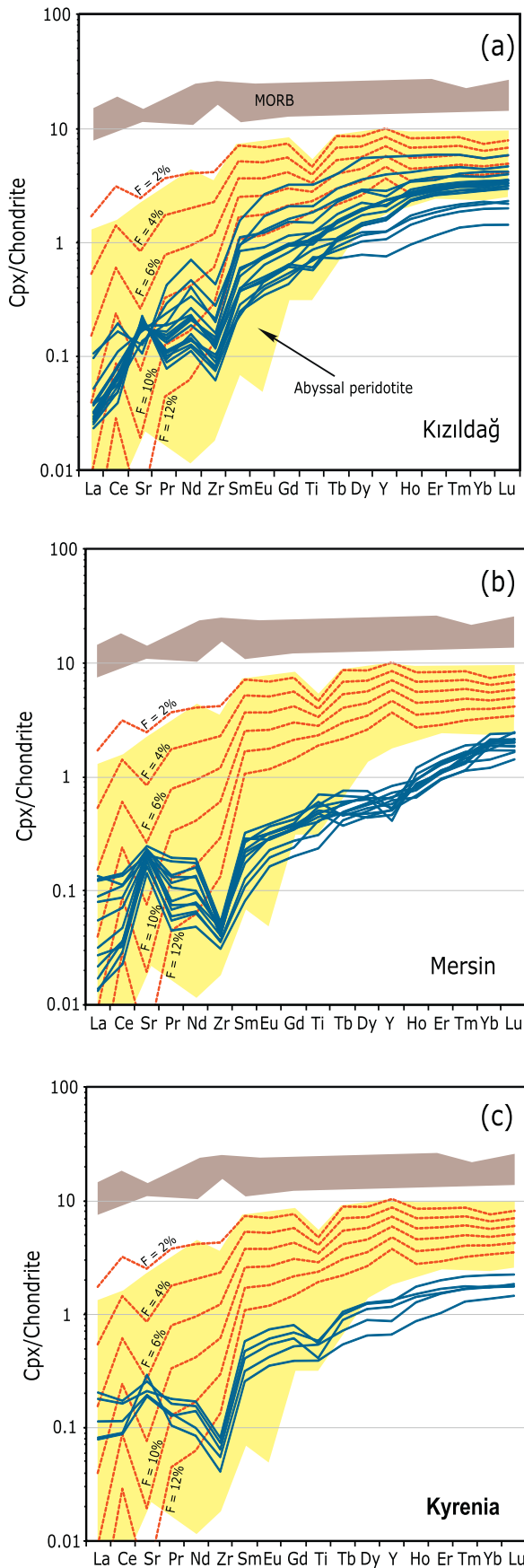(a) MORB / Abyssal peridotite / Kızıldağ

Fig. 6. Plot of clinopyroxene Yb vs. spinel Cr# for the peridotites. Theoretically calculated melting trajectories were obtained as a combination of changing the compositions of residual clinopyroxene (Johnson et al., 1990) and spinel (Hellebrand et al., 2001) with degree of melt extraction, assuming the depleted MORB source as an initial composition (Salters and Stracke, 2004). Dashed curve corresponds to anhydrous melting where melting is dominated by clinopyroxene consumption, while solid curve represents hydrous melting characterized by increased rate of orthopyroxene melting.

Stracke, 2004; Snow and Reisberg, 1995). Although $^{187}Os/^{188}Os$ values of the samples cluster mostly around 0.117–0.120, there are some samples characterized by higher $^{187}Os/^{188}Os$ values (0.120 to 0.125), which may indicate involvement of melts or fluids from sources with more radiogenic Os isotopic signatures.

5. Discussion

5.1. Mantle region characteristics

The ophiolite suites investigated here were previously defined as SSZ-type, as several lines of evidence indicate that they represent lithospheric mantle formed in close proximity to a subduction system (Bağcı et al., 2005; Dilek and Thy, 2009; Morris et al., 2017; Parlak et al., 1996). In this study, fO_2 values of peridotites of $-0.2 < FMQ < +1.5$ were calculated on the basis of Fe/Mg olivine-spinel exchange. The majority of samples having equilibrated at 0.5 to 1.5 log unites above FMQ, which may indicate that the peridotites characterize a mantle region that was more oxidized than the estimated range for the present-day reduced upper mantle represented by abyssal peridotites and MORB lavas (e.g., Aldanmaz et al., 2009; Kelley and Cottrell, 2009). On a classical $\Delta logf^{FMQ}O_2$ vs. spinel Cr# diagram (Fig. 8) the samples plot mostly on the oceanic arc peridotite compositional space, suggesting that subduction-related processes increased the redox budget of the mantle wedge by imparting a variable quantity of oxidized material into the mantle during fluid transport (e.g., Kelley and Cottrell, 2009).

(b) MORB / Mersin

(c) MORB / Kyrenia

Fig. 5. Normalized trace element patterns of residual clinopyroxenes for the peridotites (solid lines). Dashed lines represent the theoretically calculated residual clinopyroxene compositions for 2 to 12% of melt extraction. The theoretical lines are defined for a spinel-lherzolite using the non-modal fractional melting approach (Johnson et al., 1990), with mode [and melt mode] of $ol_{0.57[0.10]} + opx_{0.27[0.20]} + cpx_{0.14[0.68]} + sp_{0.02[0.02]}$ (Aldanmaz et al., 2009). The initial source is assumed to be equivalent to the hypothetical depleted MORB mantle composition of Salters and Stracke (2004). Abyssal peridotite field is based on the data from Johnson et al. (1990), Johnson and Dick (1992), Hellebrand et al. (2001) and Warren (2016).
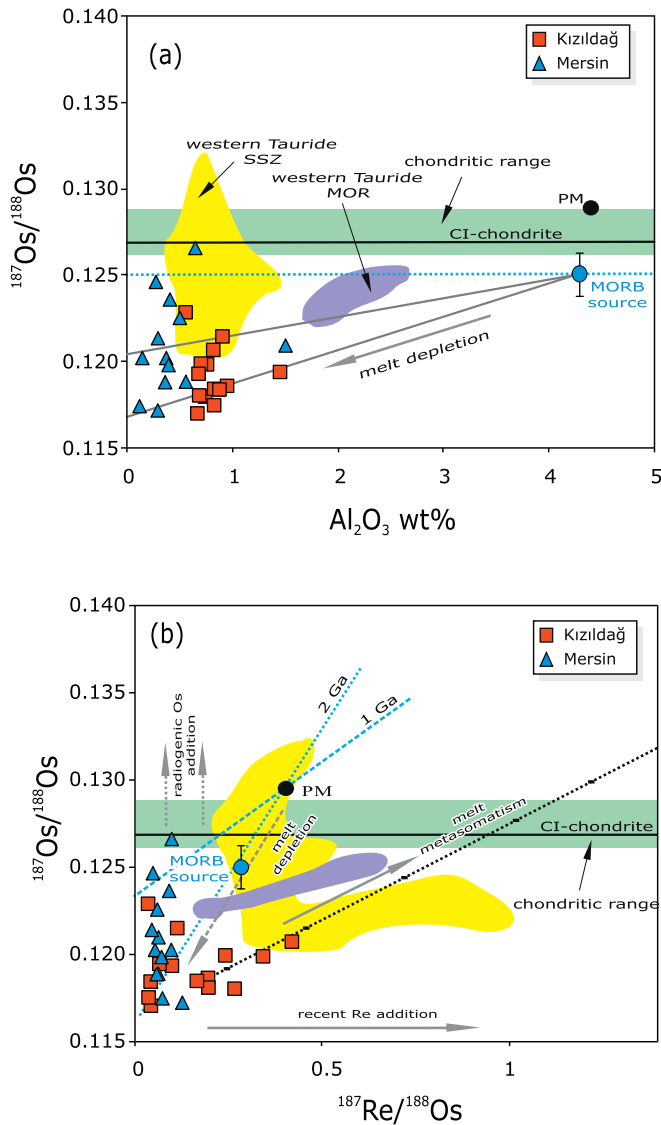
Fig. 8. Variations of $\Delta\log fO_2^{(FMQ)}$ with spinel Cr# for the peridotites. Oxygen fugacity values were estimated employing the oxygen barometer of Ballhaus et al. (1991). The ferric iron contents of the spinels used for the calculations were estimated from electron micro probe data utilizing secondary standardization (Davis et al., 2017). The compositional fields for the ocean ridge, oceanic arc and passive margin peridotites are from Parkinson and Pearce (1998), while those for the peridotites from western Tauride ophiolites are from Aldanmaz et al. (2009).

Fig. 7. Bulk-rock $^{187}Os/^{188}Os$ variations with (a) Al_2O_3 contents and (b) $^{187}Re/^{188}Os$ ratios for the peridotites from the Kızıldağ and Mersin ophiolites. Estimates compositions for the MORB source and the primitive mantle compositions are from Salters and Stracke (2004) and Meisel et al. (1996), respectively. The compositional field for carbonaceous chondrites (Meisel et al., 1996) and the average value for CI-chondrite (Luck and Allègre, 1983) are also shown comparison. The compositional fields for the peridotites from western Tauride ophiolites are based on data from Aldanmaz et al. (2012). 1 and 2 Ga geochrons were defined relative to primitive mantle using the isotopic values and parameters given in Meisel et al. (1996) and Aldanmaz et al. (2012).

Supra-slab mantle regions are generally characterized by strong isotopic heterogeneity that is interpreted to signify the combined and contrasting effects of long-term melt depletion and recycled material addition (Elliott et al., 1997). Osmium isotopic diversities recorded in mantle wedge peridotites are interpreted to reflect the effects of variable processes including, re-melting of ancient *Re*-depleted mantle material, the long-term preservation of old platinum group element-rich alloys in the upper mantle, or the modification of the mantle Os isotopic signature by interaction with metasomatic slab components (Aldanmaz et al., 2012; Senda et al., 2016).

The differential effects of slab components in creating Os isotopic heterogeneity in distinct parts of a subduction system are generally ascribed to a disparity in the behavior of Os at discrete mantle conditions. Results from some previous studies have shown that the mobility of Os in subduction zones varies significantly and is mainly dependent on the
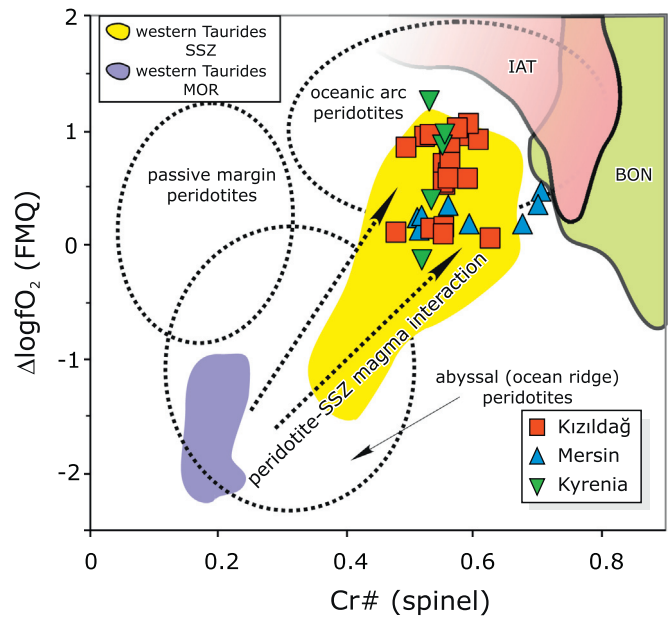
stability of sulfides in the descending slab, which is controlled primarily by the depth of dehydration reactions (e.g., Tomkins and Evans, 2015). Cr-spinels from boninitic rocks, for instance, have been shown to have $^{187}Os/^{188}Os$ ratios that are comparable to those recorded in abyssal peridotites (e.g., Suzuki et al., 2011), and this may indicate the limited contribution of crust-derived Os in the shallow fore-arc mantle, which is considered to be the main source of boninitic melts. Liu et al. (2018) further suggested that Os is relatively immobile in fluids released from the descending slab in shallow depths in the fore-arc mantle and is more mobile in slab-derived silicate melts or supercritical fluids at greater depths in mantle wedge.

The peridotites we investigate here exhibit a relatively large range of Os isotopic ratios with γOs values of between −7.7 and −0.2. This may be the result of compositional heterogeneities in the preexisting lithospheric mantle which likely contained old Os–Ir–Ru alloys with Os isotopic signatures that reflected variable effects of ancient melt depletion (e.g., Aldanmaz et al., 2012), or for a relatively limited number of samples in which slightly more radiogenic $^{187}Os/^{188}Os$ ratios were recorded, may indicate the effects of melt involvement from the sublithospheric lower part of a mantle wedge with a MORB-source like Os isotopic signature (Fig. 7). The samples, however, are all characterized by sub-chondritic $^{187}Os/^{188}Os$ ratios. This indicates that they represent a mantle region with significantly low time-integrated Re/Os, which is likely to be associated with ancient melt depletion. The samples also record $^{187}Os/^{188}Os$ that is less radiogenic than those proposed for the depleted MORB mantle and typical arc mantle sources (Fig. 7), indicating the long-term isotopic evolution of a reservoir that possessed a depleted Re/Os signature and exhibited no significant effect of recycled material with radiogenic ^{187}Os. These characteristics suggest that the peridotites are the relics of a lithospheric mantle that remained isolated from mantle convection for a long period of time, and that they probably represent a shallow fore-arc mantle, where contribution from slab-derived radiogenic Os is restricted by the increased stability of sulfides (Liu et al., 2018; Tomkins and Evans, 2015).

5.2. Extent of partial melting

Partial melting above subducting plates is known to involve hydrous fluxing of supra-slab mantle, which causes a large degree of melting of mantle wedge peridotites (Grove et al., 2012). The petrographic evidence presented above suggests that the highly refractory peridotites from the ophiolite bodies studied here are likely to be the residues of moderate to high-degrees of partial melting. This is, to the first order, consistent with the high spinel Cr# (0.47–0.75) that indicates that the peridotites have experienced higher degrees of melting (~16%–20%) than that recorded in typical ocean ridge settings (e.g., Aldanmaz et al., 2009; Hellebrand et al., 2001; Warren, 2016).

The effects of the variable extent of partial melting on the chemistry of the mantle rocks can be best traced using the relative abundances of incompatible elements in the residual silicate minerals. Clinopyroxene, in particular, is known to be alteration resistant, and even in highly serpentinized mantle rocks the abundances of relatively immobile trace elements in residual clinopyroxenes offer important information in identifying the type and extent of melt depletion (e.g., Aldanmaz et al., 2009; Birner et al., 2017; Bizimis et al., 2000; Johnson et al., 1990). Fig. 9 shows a comparison of theoretically calculated melt depletion trends with variations in HFSE and HREE in the clinopyroxenes in an attempt to quantify the degree of partial melting. The melting trajectories shown were determined using the fractional melting approach using parameters described in Shervais and Jean (2012), and with the initial source assumed to be equivalent to the hypothetical DMM (depleted MORB mantle; e.g., Salters and Stracke, 2004).

The results show a significant correlation between Ti and Dy abundances, and this may indicate that both elements behaved coherently during melt extraction. There are, however, some distinctions between the clinopyroxenes from the different ophiolite suites in terms of their absolute concentrations of trace elements. Clinopyroxenes from the Mersin and Kyrenia range ophiolites are generally characterized by relatively restricted ranges of trace element concentrations. Very low concentrations of Ti and Dy in these samples may be modeled by moderate to high degrees of melt extraction from the inferred DMM source
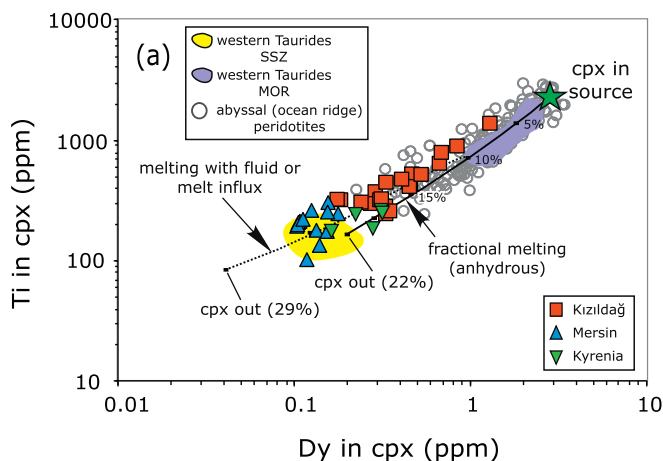

Fig. 9. Plot of Ti vs. Dy for residual clinopyroxenes from the peridotites compared with model melting trajectories drawn for melting of a spinel peridotite under anhydrous (solid lines) and hydrous (dashed lines and curves) conditions. The modeling utilizes the non-modal fractional melting equation (Johnson et al., 1990) with mineral/matrix partition coefficients compiled from Johnson et al. (1990), McKenzie and O'Nions (1991) and Kimura and Kawabata (2014). Anhydrous melting refers to the model in which melting is dominated by clinopyroxene consumption (with mode [and melt mode] of $ol_{0.55[0.10]} + opx_{0.26[0.20]} + cpx_{0.15[0.68]} + sp_{0.02[0.02]}$), and all clinopyroxene is exhausted at 22% melting, while in hydrous melting, increased rate of orthopyroxene consumption causes melting to continue in the presence of clinopyroxene until 29% melting (with mode [and melt mode] of $ol_{0.55[-0.17]} + opx_{0.32[0.65]} + cpx_{0.11[0.47]} + sp_{0.02[0.05]}$). Data sources for the abyssal peridotites field are as in Fig. 5.

(Fig. 9). In these two suites significant depletion of incompatible trace elements in the residual clinopyroxenes is probably a result of hydrous melting of peridotite, rather than simple dry melting during which clinopyroxene disappears at ~22% melting (e.g., Johnson et al., 1990). The appearance of clinopyroxene as one of the residual phases in these refractory mantle representatives may further indicate that mantle influx by a hydrous melt or fluid facilitated greater extent of orthopyroxene dissolution and allowed melting to be sustained in the presence of residual clinopyroxene toward high melting degrees (Aldanmaz et al., 2009; Grove et al., 2012).

Clinopyroxenes from the Kızıldağ ophiolite, on the other hand, exhibit much larger variations in Ti and REE abundances, and this may suggest that they represent a mantle region with a more complex petrogenetic history (Figs. 5, 9). This suite of ophiolite contains samples with low clinopyroxene Ti and Dy abundances indicating moderate to high degrees of partial melting (>15%) and an origin similar to those from the Mersin and the Kyrenia range ophiolites. However, within the same suite, there are also samples with clinopyroxene Ti and Dy abundances as high as those reported for the majority of abyssal (or mid-ocean ridge-type) peridotites that are interpreted to be the solid residues of relatively small-degrees of partial melting (<10%; Johnson et al., 1990; Aldanmaz et al., 2009; Liang and Liu, 2016). Such high abundances of trace elements in the residual clinopyroxenes of the Kızıldağ ophiolite are unlikely to be attributed to a low-degree of partial melting because their refractory modal compositions and considerably high spinel Cr/Al ratios require relatively high-degrees of melt extraction.

The elevated trace element concentrations in clinopyroxenes from the Kızıldağ ophiolite suggest that some portions of the mantle section in this suite have experienced element redistribution during melt movement. Melt-residue interaction is known to be operational during melt transport, and its effects are generally reflected by a change in modal mineralogy and composition of the residual minerals (Batanova et al., 2011; Johnson et al., 1990; Rampone et al., 2008). In the Kızıldağ suite, the melt-metasomatized peridotites that contain clinopyroxenes enriched in incompatible trace elements are also distinguished by their anomalously high spinel Ti contents, suggesting that after their strong, hydrous melt/fluid-fluxed melt depletion, some regions of the supra-slab mantle experienced metasomatic enrichments through interaction with melts rich in incompatible elements.

5.3. Melt-rock interaction during open system melting

The mantle rocks investigated here represent mantle regions with clear signs of metasomatic alteration. Our estimates for the degree of partial melting suggest that the peridotites are the solid residues of ~16 to 20% of melt extraction. However, all three ophiolite suites contain samples with a modal olivine content that is much greater than may be modeled by our estimates of the degree of partial melting. This is likely a consequence of melt-rock interaction that, in many cases, results in the formation of modally metasomatized mantle domains (Kelemen et al., 1992; Niu, 2004). The formation of olivine-rich residues is particularly common in supra-subduction mantle regions where interaction with hydrous melts leads to an increased depletion of the residue through a process involving incongruent melting of orthopyroxene and precipitation of olivine in conjunction with the production of Si-rich melt (Batanova et al., 2011; Kubo, 2002; Rampone et al., 2008).

The effects of metasomatic alterations in mantle rocks are well documented by variations in the chemical compositions of residual minerals (e.g., Aldanmaz et al., 2009; Dick and Bullen, 1984; Hellebrand et al., 2001; Johnson et al., 1990; Pearce et al., 2000). Gallium, in particular, is suggested to have low diffusivity in mantle minerals, and hence its content remains largely unchanged during cooling and re-equilibration (Dare et al., 2009). Its concentration in spinel therefore can be used in combination with Fe^{+3} and Cr# of spinel to provide insights into the possible effects of interaction of mantle rocks with
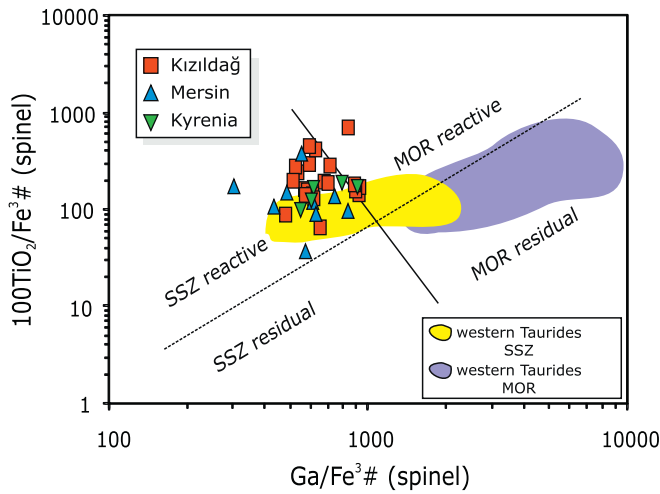
Fig. 10. $TiO_2/Fe^3\#$ vs. $Ga/Fe^3\#$ variations in peridotite spinels. The lines defining the fields for different types of peridotites are from Dare et al. (2009).

melts of different origins, as well as the nature and provenance of melt generation.

Compositional variations in spinels are shown on a $100*TiO_2/Fe^{+3}\#$ vs. $Ga/Fe^{+3}\#$ plot, on which the separate fields represent compositionally distinct mantle residues from different tectonic settings (Dare et al., 2009). The spinels analyzed during this study generally have lower $Ga/Fe^{+3}\#$ ratios compared to peridotite spinels from mid-ocean ridge settings (shown as MOR residues). Since the $Ga/Fe^{+3}\#$ ratio is not affected to a large extent by magmatic differentiation, the variation in this ratio is unlikely to be related to the change in the degree of partial melting, although the redox dependence of Fe^{+3} makes it possible to use this ratio to discriminate between MOR residues and the higher $Fe^{+3}\#$ SSZ residues. The variations in the spinel $Ga/Fe^{+3}\#$, when combined with $TiO_2/Fe^{+3}\#$, can therefore be used to identify the effects of melt-solid reactions because during interaction with percolating silicate melt, $Ga/Fe^{+3}\#$ ratio in residual spinel decrease while $TiO_2/Fe^{+3}\#$ increase or remain constant (Aldanmaz, 2012; Dare et al., 2009). As shown in Fig. 10 the peridotites we investigate plot entirely on the SSZ reacted field, indicating that the compositional variations in these mantle residues are at least partly the result of melt-rock interaction.

A complementary piece of evidence for the reactive origin of the peridotites comes from the compositions of residual clinopyroxenes which exhibit trace element patterns that cannot be reproduced by applying a simple fractional melting model (Fig. 11). Although the low absolute abundances of HREE and HFSE in clinopyroxenes are consistent with the highly depleted nature of these residues (Fig. 9), the majority of the clinopyroxene grains display fractionated incompatible element ratios (e.g., Ti/Zr and Ti/Nd) when compared to the compositions of residues formed by normal ridge processes represented by the simple fractional melting trend shown in Fig. 11. Such element fractionations, which require selective enrichments in more incompatible over less incompatible elements, cannot be modeled by simple melting and instantaneous melt removal, but most likely require open system melting during which fluid influx or interaction with percolating melts modify the composition of the residue.

Subduction influx in supra-slab mantle regions is known to create metasomatic domains with particular concentration increases in subduction-mobile incompatible elements (Shervais and Jean, 2012). This is largely the result of continuous addition of subducted material that would prevent significant depletion of the source in subduction-mobile elements as melting proceeds. The modeling in Fig. 11a show that fluid influx has the potential to explain the higher LREE/HFSE ratios of residual clinopyroxenes compared to the residue compositions from
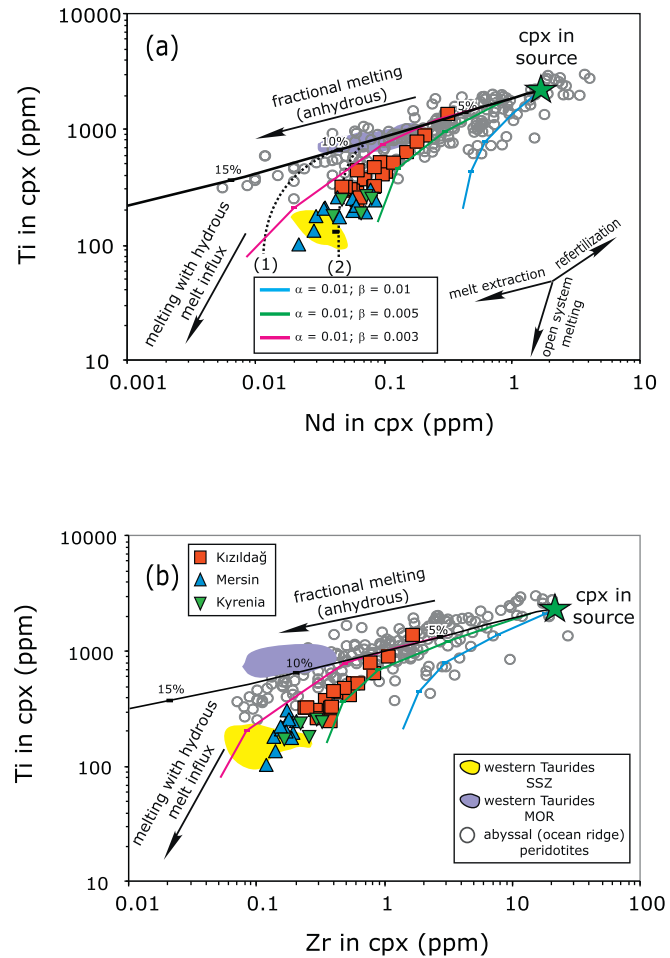

Fig. 11. (a) Ti vs. Nd and (b) Ti vs. Zr variations for residual clinopyroxenes from the peridotites to illustrate the effects of simple fractional melting (anhydrous), fluid induced melting of a depleted peridotite (dashes curves) and melting by hydrous melt influx (colored curves). Anhydrous melting assumes simple fractional melting of lherzolite and uses the parameters described in Fig. 9. Hydrous melting refers to fluid assisted re-melting of previously depleted peridotite and involves continues addition of fluid mobile incompatible trace elements to the source. The melting trajectories for hydrous melting are calculated using the parameters presented in Shervais and Jean (2012) with the concentration range of trace elements in the fluid components as given in Aldanmaz et al. (2009) (for the curves (1) and (2): Ti = 0–436; Nd = 1.1–22.2 ppm). The trajectories for melting with melt influx are drawn using the open system melting equation of Ozawa (2001), assuming a range of melt influx rates (β) and a constant mass ratio of retained melt in the residue (α). Calculations for open-system melting are designated to be dominated by incongruent dissolution of orthopyroxene (with mode [and melt mode] of $ol_{0.60[-0.17]} + opx_{0.29[0.65]} + cpx_{0.09[0.47]} + sp_{0.02[0.05]})$ and involve depleted peridotite and primary arc tholeiitic melt (with Ti, Nd and Zr compositions of 1829, 0.79 and 18 ppm, respectively) as the initial bulk and the inflowing melt compositions, respectively. Data sources for the abyssal peridotites field are as in Fig. 5.

simple fractional melting under anhydrous conditions. However, HFSEs also display some degree of fractionation as on a Ti vs. Zr plot the majority of the residual clinopyroxenes diverge from the fractional melting trend toward lower Ti values (Fig. 11b).

This may indicate that whilst fluid influx may have some effects on the compositions of the mantle residues investigated here, it is unlikely to be a viable mechanism to create the large depletions in Ti/Zr because HFSE are unlikely to be fractionated significantly by subduction fluids (e.g., Münker et al., 2004). It appears, rather, that the compositional variations in clinopyroxenes shown in Fig. 11 require involvement of melts with fractionated trace element ratios, most probably reflecting the chromatographic effects of reactive porous flow during melt percolation (Aldanmaz et al., 2009; Rampone et al., 2008). The results of theoretical modeling in Fig. 11b therefore show that the compositional variations of

residual clinopyroxenes reflect open system behavior of mantle melting and require melt influx of the peridotite during melting.

5.4. Nature and origin of interacting melts

A large range in clinopyroxene HFSE and REE abundances suggests that more than one compositionally different melt with distinct trace element compositions was involved and changed the composition of the peridotites. The separate trends formed by different HFSE and REE abundances in Fig. 11 appear to reflect interaction of residues with distinct melt compositions rather than different melt extraction rates. Variations in the Cr# and TiO_2 concentration of spinel provides further insight into the type of metasomatic interaction and the likely composition of the melts involved. Although a Cr/Al ratio of residual spinel in mantle rock is generally interpreted to vary with the degree of melt removal, equilibration with silicate melts is also known to have an additional effect (e.g., Edwards and Malpas, 1996). The spinels from the ophiolite suites exhibit significant compositional variations on a projection of Cr# vs. TiO_2 (Fig. 12a). None of the samples follow the theoretically calculated partial melting trend obtained using simple fractional melting (Johnson et al., 1990) with the typical MORB mantle as the initial source. Instead, the peridotites deviate from the melting trajectory to higher Ti compositions and form two separate trends with different slopes. The displacement from the melting trajectory to higher Cr# and Ti contents is unlikely to be attributed to depletion by melt removal, but may be interpreted to reflect the effects of melt-peridotite reactions during which spinel has equilibrated with the interacting melt (Edwards and Malpas, 1996; Kelemen et al., 1997; Pearce et al., 2000).

The extrapolation of the trends toward lower Cr# and Ti abundance gives an approximate degree of partial melting (~14%) on the calculated melting trajectory. This, however, appears to reflect the melt extraction by simple fractional melting with no equilibration between melt and spinel in the residue, and probably corresponds to the extent of melt depletion that the preexisting oceanic lithospheric mantle had experienced prior to subduction initiation (Fig. 12a). This suggests that the different trends on the diagram need to be interpreted as resulting from a second stage melting that involves interaction of depleted peridotites with compositionally different melts including: (1) predominantly typical arc tholeiitic composition for the Kızıldağ and Kyrenia range ophiolites; and (2) boninitic composition for the Mersin ophiolite (Fig. 12b).

The observed diversity in melt chemistry appears to be consistent with heterogeneities in the compositions of the crystalline rocks that comprise the crustal sequences of the ophiolite suites in this region (Bağcı et al., 2005; Dilek and Thy, 2009). Melt products that range in composition from typical arc tholeiite to boninite have been reported from the Troodos and the Tauride belt ophiolites, and these compositional distinctions have been interpreted to reflect fore-arc evolution during subduction initiation and signify polybaric partial melting of a compositionally heterogeneous mantle column with compositional heterogeneities generally suggested to be the result of processes related to the extension of the fore-arc (e.g., Dilek and Thy, 2009; Pearce and Robinson, 2010).

5.5. Implications for the melt evolution during fore-arc spreading

The compositional diversity in melt chemistry that we find may have been partly attributed to vertical compositional variations in the melting column, with relatively fertile mantle material inflowing the wedge, or tapping of compositionally variable mantle sources in response to fore-arc spreading, but is more likely a result of the differences in the styles of melt generation in different depths of the supra-slab mantle region. Subduction initiation is usually considered to cause fluid-assisted melting of wedge peridotites that also receive a subduction component to some extent. This produces melt with subduction signatures, and leaves behind refractory peridotite as the
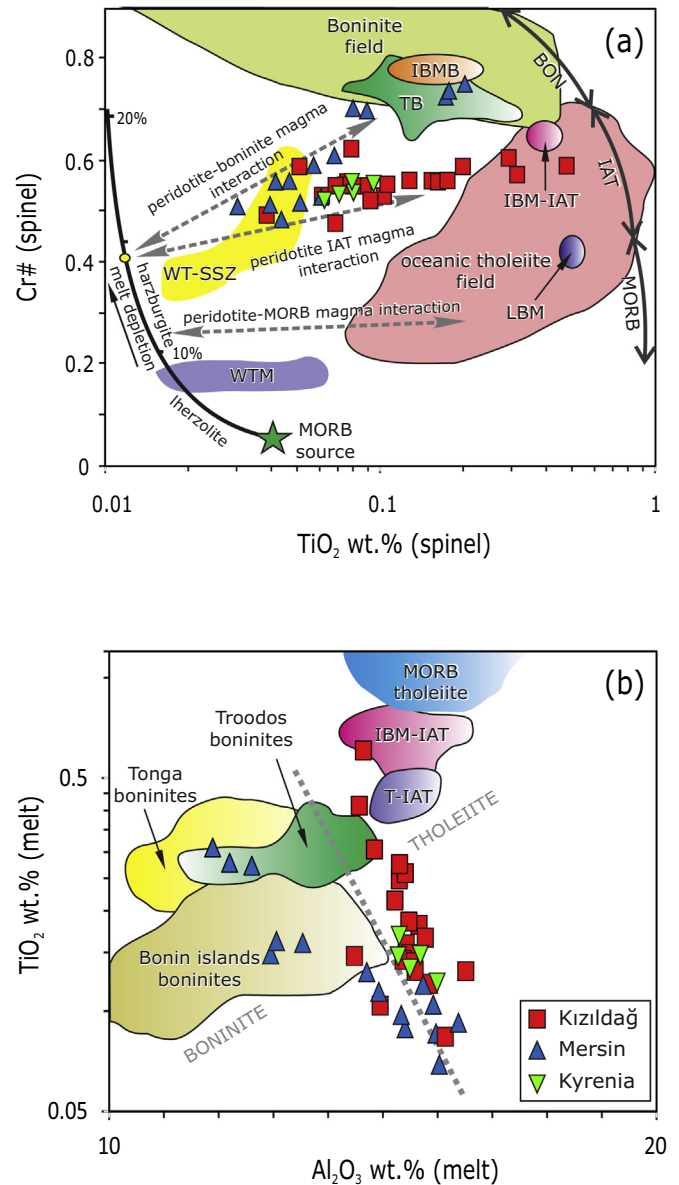

Fig. 12. (a) Plot of Cr# vs. TiO_2 in peridotite spinels highlights the effects of partial melting and peridotite - melt interaction. Heavy solid line denotes the modeled partial melting trajectory drawn using the depleted MORB source as an initial composition with the parameters defined in Pearce et al. (2000). Boninite field for the Troodos ophiolite are based on the data from Golowin et al. (2017) and references therein, while the fields for boninite and MORB fields are from the global database of Kamenetsky et al. (2001). The compositional range of spinels for mid ocean ridge basalts (MORB), island-arc tholeiites (IAT) and boninites (BON) are from Arai (1994) and Pearce et al. (2000). *Key to abbreviations:* IBMB = Izu-Bonin-Mariana boninites; IBM-IAT = Izu-Bonin-Mariana island arc tholeiite; TB = Troodos boninites; LBM = Lau Basin MORB; WT-SSZ = Western Taurides SSZ; WTM = Western Taurides MORB. (b) Calculated TiO_2 and Al_2O_3 compositions of the primary melts in equilibrium with residual spinels and clinopyroxenes. TiO_2 was calculated to be in equilibrium with the residual clinopyroxene using the mineral/melt partition coefficient given in Laubier et al. (2014), while Al_2O_3 was estimated using the spinel compositions following the approach of Rollinson (2008). Also plotted for comparison are the compositional fields for primary melts of MORB tholeiites (represented by MORB glasses; Yang et al., 2018); Izu-Bonin-Mariana island arc tholeiite - IBM-IAT (Maehara and Maeda, 2004; Schmidt and Jagoutz, 2017 and references therein); Troodos island arc tholeiite (T-IAT) and boninite (represented by fresh volcanic glasses; Regelous et al., 2014; Woelki et al., 2018); Bonin Island boninites (Dobson et al., 2006; Kanayama et al., 2012); and Tonga Arc boninites (Cooper et al., 2010).

complementary solid residue. The composition of the oceanic crust produced during subduction initiation is likely represented by tholeiitic magmas that are geochemically transitional between typical MORB

and primitive arc lavas. Depending on the amount of material transported during initial stages of subduction and on the processes during the passage of melts through the lithospheric column, the melts erupted may be represented by typical arc tholeiite or may be compositionally similar to what is defined as fore-arc basalt (e.g., Reagan et al., 2010).

For our three ophiolite cases, there appears to be a common occurrence of arc tholeiite magmas that are unlikely to be explained by melting of highly refractory sources. This suggests that the early melt production started in the mantle wedge where melting of relatively less depleted asthenospheric material was enabled most probably by the combination of mantle hydration and decompression during near trench spreading, producing primitive tholeiite melts. The resultant primary melts then migrated upward into the shallower parts of the mantle, where they reacted with the refractory peridotites of the overlying mantle lithosphere to facilitate further melting. The refractory peridotites in the shallow supra-slab mantle region, where the depleted character of the rocks has been shown by Os isotopic evidence to be a regional feature that was developed well before the time of subduction initiation, thus appear to represent the source of a second stage melting that produced melts to form oceanic crust with typical SSZ character.

This second stage melting likely occured at shallower depths, and required more water-rich melts to be involved. The addition of large volumes of melts during this later stage is probably the main cause of partial melting of the hydrated peridotite as it causes increased incongruent melting of orthopyroxene in refractory mantle (Kelemen et al., 1992; Kubo, 2002), which in turn changes the melt composition to become more silica-rich, yet more diluted in most incompatible elements (van den Bleeken et al., 2011). As is documented experimentally in some recent studies (e.g., Mitchell and Grove, 2016), reaction of depleted peridotites with a deeper melt, although resulting orthopyroxene dissolution in almost all cases, may create a large range of mantle residues from depleted dunites and harzburgites to refertilized harzburgites and wehrlites depending on the type of reaction which is basically identified by the initial melt composition and the rate of melt influx.

In the case of the ophiolite suites we examine here the samples that we interpret to have reacted with IAT-type melt appear to be the products of orthopyroxene dissolution and olivine and clinopyroxene crystallization. This indicates influx of a melt saturated in olivine + clinopyroxene, which appears to have interacted with the variably depleted harzburgites of the pre-existing lithospheric mantle to form mantle restites containing clinopyroxenes with a wide range of trace element contents. This melt also produced wehrlitic mushes which partly crystallized to form ultramafic cumulates near the base of the crust, while more differentiated melts migrated upward, forming typical IAT-type magmatic crust as is the case in the Kızıldağ Ophiolite. Alternatively, if the reacting low-silica basaltic melt, which is saturated in clinopyroxene and olivine at its source, becomes progressively olivine saturated due to the expansion of the olivine phase volume upon decompression during ascent (e.g., Rampone et al., 2008; Wagner and Grove, 1998) its interaction with harzburgite will cause greater extent of orthopyroxene dissolution and olivine precipitation, which, in turn, results in the formation of Mg- and Si-rich melt and more olivine-rich residue. This later mechanism explains the formation of melts with boninitic affinities and their corresponding residues with high modal olivine contents and incompatible element depleted clinopyroxenes.

We foresee that this second stage melting of the mantle wedge during subduction infancy, extracting arc tholeiites and boninites, created the highly depleted mantle wedge rocks of the three ophiolites of our study. These melts flowed upward into the supra-subduction zone spreading center and produced SSZ ophiolitic crust, which contains a range of compositionally diverse magmatic products reflecting the effects of different types of reaction processes between deeper melt and previously depleted peridotites of the pre-existing oceanic lithosphere. The spreading of the overriding lithosphere as a result of tectonically accommodated fore-arc extension then resulted in the exposure of the mantle rocks at the seafloor causing also ophiolite dismemberment.

6. Conclusions

The mantle representatives from the Cretaceous Neotethyan ophiolites in southern Turkey and Northern Cyprus display geochemical signatures indicative of complex petrogenetic processes including partial melting and melt-rock interaction in a supra-slab mantle region. The peridotites exhibit highly variable, but generally sub-chondritic $^{187}Os/^{188}Os$ ratios. Although there are some samples with Os isotopic signatures indicative of the effects of interaction with melts from sub-lithospheric sources, the depleted $^{187}Os/^{188}Os$ compared to the ambient oceanic upper mantle ($^{187}Os/^{188}Os$ ~0.127) for all the samples suggest that they represent a mantle lithosphere with signatures of ancient melt depletion.

Chemical variations in the primary minerals suggest that the peridotites have experienced two stages of melt depletion. The first appears to be an inherited feature from the earlier formation of the mantle lithosphere through crust-mantle segregation along a mid-oceanic spreading center, while the second defines processes that involve melt generation and evolution in association with fore-arc spreading during subduction initiation. Relative abundances of incompatible trace elements in the residual clinopyroxenes and spinels suggest that the former can be described in the form of simple fractional melting, while the latter needs to be explained in context of open-system melting which involves reactive dissolution of orthopyroxene during interaction of previously depleted harzburgites of the overlying lithosphere with melts from deeper asthenospheric mantle wedge. Reacting melts appear to be hydrous and more oxidizing than typical MORB melt and are likely of arc tholeiite character.

During their upward migration, these melts reacted with the refractory peridotites of the overlying mantle lithosphere to enable further melting, which in turn created a large range of mantle residues from depleted dunites and harzburgites to refertilized harzburgites, and caused the melt composition to evolve to form typical fore arc basalt and boninite through dissolution of orthopyroxene and precipitation of olivine ($\pm$ clinopyroxene).

Declaration of Competing Interest

The authors declare that they have no known competing financial interests or personal relationships that could have appeared to influence the work reported in this paper.

Appendix A. Supplementary data

Supplementary data to this article can be found online at https://doi.org/10.1016/j.lithos.2020.105438.

References

Aldanmaz, E., 2012. Trace element geochemistry of primary mantle minerals in spinel-peridotites from polygenetic MOR–SSZ suites of SW Turkey: constraints from an LA-ICP-MS study and implications for mantle metasomatism. Geol. J. 47, 59–76.

Aldanmaz, E., Schmidt, M.W., Gourgaud, A., Meisel, T., 2009. Mid-ocean ridge and supra-subduction geochemical signatures in spinel–peridotites from the Neotethyan ophiolites in SW Turkey: Implications for upper mantle melting processes. Lithos 113, 691–708.

Aldanmaz, E., Meisel, T., Çelik, Ö., Henjes-Kunst, F., 2012. Osmium isotope systematics and highly siderophile element fractionation in spinel-peridotites from the Tethyan ophiolites in SW Turkey: implications for multi-stage evolution of oceanic upper mantle. Chem. Geol. 294–295, 152–164.

Al-Riyami, K., Robertson, A.H.F., Dixon, J., Xenophontos, C., 2002. Origin and emplacement of the late cretaceous Baer-Bassit ophiolite and its metamorphic sole in NW Syria. Lithos 65, 225–260.

Arai, S., 1994. Characterisation of spinel peridotites by olivine-spinel compositional relationships: review and interpretation. Chem. Geol. 113, 191–204.

Asimow, P.D., 1999. A model that reconciles major- and trace-element data from abyssal peridotites. Earth Planet. Sci. Lett. 169, 303–319.

Bağcı, U., Parlak, O., Höck, V., 2005. Whole rock and mineral chemistry of cumulates from the Kızıldağ (Hatay) ophiolite (Turkey): clues for multiple magma generation during crustal accretion in the southern Neotethyan Ocean. Mineral. Mag. 69, 53–76.

Batanova, V., Belousov, I., Savelieva, G., Sobolev, A., 2011. Consequences of channelized and diffuse melt transport in supra-subduction zone mantle: evidence from the Voykar Ophiolite (Polar Urals). J. Petrol. 52, 2483–2521.

Birner, S.K., Warren, J.M., Cottrell, E., Davis, F.A., Kelley, F.A., Fallon, T.J., 2017. Forearc peridotites from Tonga record heterogeneous oxidation of the mantle following subduction initiation. J. Petrol. 58, 1755–1780.

Bizimis, M., Salters, V.J.M., Bonatti, E., 2000. Trace and REE content of clinopyroxenes from supra-subduction zone peridotites. Implications for melting and enrichment processes in island arcs. Chem. Geol. 165, 67–85.

Cooper, L.B., Plank, T., Arculus, R.J., Hauri, E.H., Hall, P.S., Parman, S.W., 2010. High-Ca boninites from the active Tonga Arc. J. Geophys. Res. 115, B10206.

Dare, S.A.S., Pearce, J.A., McDonald, I., Styles, M.T., 2009. Tectonic discrimination of peridotites using fO_2–Cr# and Ga-Ti-Fe^{III} systematic in chrome–spinel. Chem. Geol. 261, 199–216.

Davis, F.A., Cottrell, E., Birner, S.K., Warren, J.M., Lopez, O.G., 2017. Revisiting the electron microprobe method of spinel-olivine-orthopyroxene oxybarometry applied to spinel peridotites. Am. Mineral. 102, 421–435.

Dick, H.J.B., Bullen, T., 1984. Chromian spinel as a petrogenetic indicator in abyssal and alpine-type peridotites and spatially associated lavas. Contrib. Mineral. Petrol. 86, 54–76.

Dilek, Y., Thy, P., 2009. Island arc tholeiite to boninite melt evolution of the cretaceous Kızıldağ (Turkey) ophiolite: model for multi-stage early arc-forearc magmatism in Tethyan subduction factories. Lithos 113, 68–87.

Dobson, P.F., Blank, J.G., Maruyama, S., Liou, J.G., 2006. Petrology and geochemistry of boninite-series volcanic rocks, Chichi-Jima, Bonin Islands, Japan. Int. Geol. Rev. 48, 669–701.

Edwards, S.J., Malpas, J., 1996. Melt-peridotite interactions in shallow mantle at the East Pacific rise: evidence from ODP Site 895 (Hess deep). Mineral. Mag. 60, 191–206.

Elliott, T., Plank, T., Zindler, A., White, W., Bourbon, B., 1997. Element transport from slab to volcanic front in the Mariana arc. J. Geophys. Res. 102, 14991–15019.

Golowin, R., Portnyagin, M., Hoernle, K., Sobolev, A., Kuzmin, D., Werner, R., 2017. The role and conditions of second-stage mantle melting in the generation of low-Ti tholeiites and boninites: the case of the Manihiki Plateau and the Troodos ophiolite. Contrib. Mineral. Petrol. 172 (11–12), 104.

Grove, T.L., Till, C.B., Krawczynski, M.J., 2012. The role of H_2O in subduction zone magmatism. Annu. Rev. Earth Planet. Sci. 40, 413–439.

Hellebrand, E., Snow, J.E., Dick, H.J.B., Hoffmann, A.W., 2001. Coupled major and trace elements as indicators of extent of melting in mid-ocean-ridge peridotites. Nature 410, 677–681.

Johnson, K.T.M., Dick, H.J.B., Shimizu, N., 1990. Melting in the oceanic upper mantle: an ion microprobe study of diopsides in abyssal peridotites. J. Geophys. Res. 95, 2661–2678.

Kamenetsky, V.S., Crawford, A.J., Meffre, S., 2001. Factors controlling chemistry of magmatic spinel: an empirical study of associated olivine, Cr-spinel and melt Inclusions from primitive rocks. J. Petrol. 42, 655–671.

Kanayama, K., Umino, S., Ishizuka, O., 2012. Eocene volcanism during the incipient stage of Izu–Ogasawara Arc: Geology and petrology of the Mukojima Island Group, the Ogasawara Islands. Island Arc 21, 288–316.

Karaoğlan, F., Parlak, O., Kloetzli, U., Thöni, M., Koller, F., 2013. U–Pb and Sm–Nd geochronology of the Kızıldağ (Hatay, Turkey) ophiolite: implications for the timing and duration of suprasubduction zone type oceanic crust formation in southern Neotethys. Geol. Mag. 150, 283–299.

Kelemen, P.B., Dick, H.J.B., Quick, J.E., 1992. Formation of harzburgite by pervasive melt/rock reaction. Nature 358, 635–641.

Kelemen, P.B., Hirth, G., Shimizu, N., Spiegelman, M., Dick, H.J.B., 1997. A review of melt migration processes in the adiabatically upwelling mantle beneath oceanic spreading ridges. Philos. Trans. R. Soc. London A 355 (1723), 283–318.

Kelley, K.A., Cottrell, E., 2009. Water and the oxidation state of subduction zone magmas. Science 325, 605–607.

Kimura, J.-I., Kawabata, H., 2014. Trace element mass balance in hydrous adiabatic mantle melting: the Hydrous Adiabatic Mantle Melting Simulator version 1 (HAMMS1). Geochem. Geophys. Geosyst. 15, 2467–2493.

Kubo, K., 2002. Dunite formation processes in highly depleted peridotite: case study of the Iwanaidake Peridotite, Hokkaido, Japan. J. Petrol. 43, 423–448.

Laubier, M., Grove, T.L., Langmuir, C.H., 2014. Trace element mineral/melt partition-ing for basaltic and basaltic andesitic melts: an experimental and laser ICP-MS study with application to the oxidation state of mantle source regions. Earth Planet. Sci. Lett. 392, 265–278.

Liang, Y., Liu, B., 2016. Simple models for disequilibrium fractional melting and batch melting with application to REE fractionation in abyssal peridotites. Geochim. Cosmochim. Acta 173, 181–197.

Liu, C.Z., Xu, Y., Wu, F.Y., 2018. Limited recycling of crustal osmium in forearc mantle during slab dehydration. Geology 46, 239–242.

Luck, J.M., Allègre, C.J., 1983. ^{187}Re–^{187}Os systematics in meteorites and cosmochemical consequences. Nature 302, 130–132.

Maehara, K., Maeda, J., 2004. Evidence for high-Ca boninite magmatism from Paleogene primitive low-K tholeiite, Mukoujima, Hahajima Island group, southern Bonin (Ogasawara) forearc, Japan. Island Arc 13, 452–465.

Maffione, M., van Hinsbergen, D., de Gelder, G., van der Goes, F., Morris, A., 2017. Kinematics of late cretaceous subduction initiation in the Neo-Tethys Ocean re-constructed from ophiolites of Turkey, Cyprus, and Syria. J. Geophys. Res. Solid Earth 122. https://doi.org/10.1002/2016JB013821.

McKenzie, D.P., O'Nions, R.K., 1991. Partial melt distribution from inversion of rare earth element concentrations. J. Petrol. 32, 1021–1991.

McPhee, P.J., Van Hinsbergen, D.J.J., 2019. Tectonic reconstruction of Cyprus reveals late Miocene Continental Collision between Africa and Anatolia. Gondw. Res. 68, 158–173.

Meisel, T., Fellner, N., Moser, J., 2003. A simple procedure for the determination of platinum group elements and rhenium (Ru, Rh, Pd, Re, Os, Ir and Pt) using ID-ICPMS with an inexpensive on-line matrix separation in geological and environmental materials. J. Anal. At. Spectrom. 18, 720–726.

Meisel, T., Walker, R.J., Morgan, J.W., 1996. The osmium isotopic composition of the Earth's primitive upper mantle. Nature 383, 517–520.

Mitchell, A.L., Grove, T.L., 2016. Experiments on melt–rock reaction in the shallow mantle wedge. Contrib. Mineral. Petrol. 171, 107. https://doi.org/10.1007/s00410-016-1312-2.

Moix, P., Beccaletto, L, Kozur, H.W., Hochard, C., Rosselet, F., Stampfli, G.M., 2008. A new classification of the Turkish terranes and sutures and its implication for the paleotectonic history of the region. Tectonophysics 451, 7–39.

Moix, P., Beccaletto, L., Masset, O., Kozur, H., Dumitrica, P., Vachard, D., Martini, R., Stampfli, G., 2011. Geology and correlation of the Mersin Mélanges, Southern Turkey. Turkish J. Earth Sci. 20, 57–98.

Morris, A., Anderson, M.W., Omer, A., Maffione, M., van Hinsbergen, D.J.J., 2017. Rapid fore-arc extension and detachment-mode spreading following subduction initiation. Earth Planet. Sci. Lett. 478, 76–88.

Münker, C., Wörner, G., Yogodzinski, G., Churikova, T., 2004. Behavior of high field strength elements in subduction zones: constraints from Kamchatka–Aleutian arc lavas. Earth Planet. Sci. Lett. 224, 275–293.

Niu, Y., 2004. Bulk-rock major and trace element compositions of abyssal peridotites: implications for mantle melting, melt extraction and post-melting processes beneath mid-ocean ridges. J. Petrol. 45, 2423–2458.

O'Driscoll, B., Walker, R.D., Day, J.M.D., Ash, R.D., Daly, J.S., 2015. Generations of melt extraction, melt-rock interaction and high-temperature metasomatism preserved in peridotites of the ~497 Ma Leka Ophiolite complex, Norway. J. Petrol. 56, 1797–1828.

Ozawa, K., 2001. Mass balance equations for open magmatic systems: trace element behavior and its application to open system melting in the upper mantle. J. Geophys. Res. 106, 13407–13434.

Parkinson, I.J., Pearce, J.A., 1998. Peridotites from the Izu-Bonin-Mariana forearc (ODP Leg 125): evidence for mantle melting and melt-mantle interaction in a supra-subduction zone setting. J. Petrol. 39, 1577–1618.

Parlak, O., Delaloye, M., 1999. Precise $^{40}Ar/^{39}Ar$ ages from the metamorphic sole of the Mersin ophiolite (southern Turkey). Tectonophysics 301, 145–158.

Parlak, O., Robertson, A.H.F., 2004. The ophiolite-related Mersin Mélange, southern Turkey: its role in the tectonic–sedimentary setting of Tethys in the Eastern Mediterranean region. Geol. Mag. 141, 257–286.

Parlak, O., Delaloye, M., Bingöl, E., 1996. Mineral chemistry of ultramafic and mafic cumulates as an indicator of the arc-related origin of the Mersin ophiolite (southern Turkey). Geologische Rundschau 85, 647–661.

Parlak, O., Karaoğlan, F., Rızaoğlu, T., Klötzli, U., Koller, F., Billor, Z., 2013. U–Pb and ^{40}Ar–^{39}Ar geochronology of the ophiolites and granitoids from the Tauride belt: implications for the evolution of the Inner Tauride suture. J. Geodyn. 65, 22–37.

Pearce, J.A., Robinson, P.T., 2010. The Troodos ophiolitic complex probably formed in a subduction initiation, slab edge setting. Gondw. Res. 18, 60–81.

Pearce, J.A., Barker, P.F., Edwards, S.J., Parkinson, I.J., Leat, P.T., 2000. Geochemical and tectonic significance of peridotites from the South Sandwich arc-basin system, South Atlantic. Contrib. Mineral. Petrol. 139, 36–53.

Rampone, E., Piccardo, G.B., Hofmann, A.W., 2008. Multi-stage melt-rock interaction in the Mt. Maggiore (Corsica, France) ophiolitic peridotites: microstructural and geochemical evidence. Contrib. Mineral. Petrol. 156, 453–475.

Reagan, M.K., Ishizuka, O., Stern, R.J., Kelley, K.A., Ohara, Y., Blichert-Toft, J., Bloomer, S.H., Cash, J., Fryer, P., Hanan, B.B., Hickey-Vargas, R., Ishii, T., Kimura, J.-I., Peate, D.W., Rowe, M.C., Woods, M., 2010. Fore-arc basalts and subduction initiation in the Izu-Bonin-Mariana system. Geochem. Geophys. Geosyst. 11 (3). https://doi.org/10.1029/2009GC002871 Q03X12.

Regelous, M., Haase, K., Freund, S., Keith, M., Weinzierl, C., Beier, C., Brandl, P., Endres, T., Schmidt, H., 2014. Formation of the Troodos Ophiolite at a triple junc-tion: evidence from trace elements in volcanic glass. Chem. Geol. 386, 66–79.

Robertson, A.H.F., 2002. Overview of the genesis and emplacement of Mesozoic ophiolites in the Eastern Mediterranean Tethyan region. Lithos 65, 1–67.

Robertson, A.H.F., McCay, G.A., Tasli, K., Yildiz, A., 2013. Eocene development of the northerly active continental margin of the Southern Neotethys in the Kyrenia Range, North Cyprus. Geol. Mag. 151, 692–731.

Rollinson, H., 2008. The geochemistry of mantle chromitites from the northern part of the Oman ophiolite: inferred parental melt composition. Contrib. Mineral. Petrol. 156, 273–288.

Salters, V.J.M., Stracke, A., 2004. Composition of the depleted mantle. Geochem. Geophys. Geosyst. 5 (5), Q05004.

Sayit, K., Bedi, Y., Tekin, U.K., Göncüoğlu, M.C., Okuyucu, C., 2017. Middle Triassic back-arcbasalts from the blocks in the Mersin Mélange, southern Turkey: implications for thegeodynamic evolution of the Northern Neotethys. Lithos 268, 102–113.

Schmidt, M.W., Jagoutz, O., 2017. The global systematics of primitive arc melts. Geochem. Geophys. Geosyst. 18, 2817–2854.

Senda, R., Shimizu, K., Suzuki, K., 2016. Ancient depleted mantle as a source of boninites in the Izu–Bonin–Mariana arc: evidence from Os isotopes in Cr–spinel and magnetite. Chem. Geol. 439, 100–119.

Shervais, J.W., Jean, M.M., 2012. Inside the subduction factory: fluid mobile trace elements in the mantle wedge above a subduction zone. Geochim. Cosmochim. Acta 95, 270–285.

Snow, J.E., Reisberg, L., 1995. Os isotopic systematics of the MORB mantle: results from altered abyssal peridotites. Earth Planet. Sci. Lett. 133, 411–421.

Stampfli, G., Marcoux, J., Baud, A., 1991. Tethyan margins in space and time. Palaeogeogr. Palaeoclimatol. Palaeoecol. 87, 373–409.

Stern, R.J., Reagan, M.K., Ishizuka, O., Ohara, Y., Whattam, S.A., 2012. To understand subduction initiation, study forearc crust: to understand forearc crust, study ophiolites. Lithosphere 4, 469–483.

Suzuki, K., Senda, R., Shimizu, K., 2011. Osmium behavior in a subduction system elucidated from chromian spinel in Bonin Island beach sands. Geology 39, 999–1002.

Tekin, U.K., Okuyucu, C., Sayit, K., Bedi, Y., Paula, J., Noble, P.J., Krystyn, L., Göncüoğlu, M.C., 2019. Integrated Radiolaria, benthic foraminifera and conodont biochronology of the pelagic Permian blocks/tectonic slices and geochemistry of associated volcanic rocks from the Mersin Mélange, southern Turkey: Implications for the Permian evolution of the northern Neotethys. Island Arc 28, e12286.

Thuizat, R., Whitechurch, H., Montigny, R., Juteau, T., 1981. K-Ar dating of the some infra-ophiolitic metamorphic soles from the eastern Mediterranean: New evidence for intra-oceanic thrusting before obduction. Earth Planet. Sci. Lett. 52, 302–310.

Tomkins, A.G., Evans, K.A., 2015. Separate zones of sulfate and sulfide release from subducted mafic oceanic crust. Earth Planet. Sci. Lett. 428, 73–83.

van den Bleeken, G., Müntener, O., Ulmer, P., 2011. Melt variability in percolated peridotite: an experimental study applied to reactive migration to tholeiitic basalt in the upper mantle. Contrib. Mineral. Petrol. 161, 921–945.

van Hinsbergen, D.J.J., Peters, K., Maffione, M., Spakman, W., Guilmette, C., Thieulot, C., Pluemper, O., Gurer, D., Brouwer, F.M., Aldanmaz, E., Kaymakci, N., 2015. Dynamics of intraoceanic subduction initiation: 2. Suprasubduction zone ophiolite formation andmetamorphic sole exhumation in context of absolute plate motions. Geochem. Geophys. Geosyst. 16, 1771–1785.

van Hinsbergen, D.J.J., Maffione, M., Plunder, A., Kaymakçi, N., Ganerød, M., Hendriks, B.W.H., Corfu, F., Gürer, D., de Gelder, G.I.N.O., Peters, K., McPhee, P.J., Brouwer, Fraukje M., Advokaat, E.L., Vissers, R.L.M., 2016. Tectonic evolution and paleogeography of the Kırşehir Block and the Central Anatolian ophiolites, Turkey. Tectonics 35, 983–1014.

van Hinsbergen, D.J.J., Torsvik, T., Schmid, S.M., Matenco, L., Maffione, M., Vissers, R.L.M., Gürer, D., Spakman, W., 2020. Orogenic architecture of the Mediterranean region and kinematic reconstruction of its tectonic evolution since the Triassic. Gondw. Res. 81, 79–229.

Wagner, T.P., Grove, T.L., 1998. Melt/harzburgite reaction in the petrogenesis of tholeiitic magma from Kilauea volcano, Hawaii. Contrib. Mineral. Petrol. 131, 1–12.

Warren, J.M., 2016. Global variations in abyssal peridotite compositions. Lithos 248–251, 193–219.

Woelki, D., Regelous, M., Haase, K.M., Romer, R.H.W., Beier, C., 2018. Petrogenesis of boninitic lavas from the Troodos Ophiolite, and comparison with Izu–Bonin–Mariana fore-arc crust. Earth Planet. Sci. Lett. 498, 203–214.

Yang, S.Y., Humayun, M., Salters, V.J.M., 2018. Elemental Systematics in MORB Glasses from the Mid-Atlantic Ridge. Geochem. Geophys. Geosyst. 19, 4236–4259.